Mechanics & Industry **26**, 5 (2025)

https://doi.org/10.1051/meca/2025001

Mechanics & Industry

Available online at:
www.mechanics-industry.org

ORIGINAL ARTICLE OPEN ACCESS

Dynamic analysis of crank slider mechanism considering 3D translational joint clearance based on variable contact area

Yuan Wang[1,2,*], Liu Juan[1,2], Ning Fengping[2], Chai Chao[2], Zhang Lei[2], and Li Hui[3]

[1] Department of Mechanical Engineering, Shanxi Engineering Vocational College, Taiyuan 03001, China
[2] College of Mechanical Engineering, North University of China, Taiyuan 030051, China
[3] Mining Engineering Department, Lvliang College, Lvliang 033001, China

Received: 26 July 2024 / Accepted: 9 January 2025

Abstract. This study investigates the influence of joint clearance on the motion accuracy of the slider in the 3D translational pair of the crank slider mechanism. Typically, joint clearance in the kinematic pair can affect the motion accuracy, stability, and service life of multibody mechanical system. The focus of this article is on the 3D translational pair, providing a detailed classification of the contact area between the slider and the guide rail. It summarizes 11 potential contact forms that may occur between these two components. Analyzing the contact states between the slider and guide rail in the 3D translational pair, the study explores three possible contact modes. Based on the geometric characteristics of the contact area between the slider and the guide rail, the mathematical expression for contact stiffness is redefined, considering both front and side contact of the contact area. Combining traditional contact force models with new contact stiffness models, a contact force model between the slider and the guide rail in a 3D translational pair is established, and the dynamics chaotic phenomena of the 3D crank slider mechanism were analyzed. The results indicate that the size of the clearance in the crank slider mechanism and the driving speed of the mechanism are the main factors affecting the dynamics and chaotic phenomena of the mechanism.

Keywords: 3D translational pair / variable contact area / joint clearance / contact mode / crank slider mechanism

1 Introduction

With the development of modern science and technology and the innovation of industrial technology, the motion accuracy, working stability and other performance indicators of multibody mechanical systems have become increasingly crucial. The quality of these key indicators depends on the mechanical material properties, geometric dimensions accuracy and the assembly precision of the system itself. As a pivotal component within links in multibody mechanical system, the accuracy of the kinematic pair directly determines the motion accuracy and working stability of the system. However, due to the manufacturing errors of mechanical components, fatigue losses during motion, and assembly precision, joint clearances in the kinematic pairs cannot be ignored, and the impact of joint clearances on the motion performance of the system is inevitable [1,2].

In multibody mechanical system, kinematic pairs are generally classified into revolute pairs, translational pairs and spherical pairs, each exhibiting varying degrees of joint clearances. Over an extended period, numerous researchers have undertaken various studies on joint clearance using different theories and technical approaches.

Liu et al. [3] conducted a study on the joint clearance of cylindrical pairs through finite element analysis. By introducing contact area, pressure distribution, maximum sustainable load, and finite element analysis results of the main components of cylindrical pairs, they established an approximate contact model for cylindrical pairs with joint clearance. The approximate model was then used to analyze the kinematics and dynamics of cylindrical pairs. Chaker et al. [4] studied the kinematic characteristics of the cylindrical pairs in a 3-RRC parallel mechanism when joint clearance is present. They used screw theory to derived the pose error of parallel mechanism's moving platform, indicating that joint clearance in cylindrical pairs has the greatest impact on the platform pose when the mechanism is in singular configurations.

* e-mail: wy15340696897@163.com

Imed Khemili et al. [5] focused on the joint clearance of the planar revolute pair in planar crank slider mechanism. They compared the dynamics of the rigid links and the flexible links when the joint clearance was in the revolute pair. Erkaya et al. [6] utilized genetic algorithms to study joint clearance of revolute pairs, using four-bar linkage mechanism as the subject of their research. Treating joint clearance as a massless virtual link, they derived its motion expression though Lagrange equation. Genetic algorithm were employed to optimize the joint clearance, achieving the optimization of the error between the desired and actual paths of the revolute pair. Flores et al. [7] introduced a dynamic modeling approach for revolute pairs in the presence of lubricants, using the revolute joint in the crank slider mechanism as an example. They investigated different hydrodynamic lubrication models, demonstrating the effectiveness of their dynamic modeling approach. Qi et al. [8] proposed a frictional contact analysis method for rigid multibody system with spatial translational joints. They proved that all contacts in the joint could be transformed into point-to-point contact form using the integration concept. They introduced two cleance functions at each contact point, determining the contact force magnitude in the contact area. Zhao et al. [9] focused on the joint clearance of revolute pairs and studied the motion accuracy of a spatial robot manipulator when subjected to joint clearance. They conducted dynamic simulation on the dynamic characteristics of a spatial robot manipulator with joint clearance.

Wang et al. [10] proposed an improved mathematical expression for contact stiffness based on the coupling relationship between the contact stiffness of two colliding objects and the mechanical system. They introduced this contact stiffness into a spatial four bar mechanism with joint clearance in spherical pair and used finite element analysis to calculate the contact force inside the spherical pair, further illustrating the impact of joint clearance on the dynamic performance of the system.

Flores et al. [11] discussed the joint clearance of translational pair and proposed that the generalized contact stiffness expression for contact between two bodies would no longer be applicable when the contact surfaces are not cylindrical or spherical. They derived a generalized contact stiffness expression suitable for two plane contact and extensively analyzed and discussed the dynamics of a planar crank-slider mechanism with joint clearance in the translational pair. Zhuang et al. [12] treated the geometric constraints of translational pairs as bilateral constraints and applied non-smooth multibody dynamics theory to study the joint clearance in translational pairs with both driving constraints and friction. They classified the contact between the slider and the guide rail into 9 cases, and introduced a Horizontal Linear Complementarity Problem (HLCP) theory, and characterized the normal force, driving force and constraint force on the slider using this theory. They designed a sliding rod mechanical mechanism with driving constraints and validated the effectiveness of the Horizontal Linear Complementarity Problem (HLCP) theory.

Wu et al. [13] addressed the issue of joint clearance in translational pairs and proposed that inclined collisions are more universal than direct collisions. Through the study of the double-crank slider mechanism, they summarized that the contact area between the slider and the guide rail in translational pair includes rectangle, triangle and point (sphere) shapes. They derived the contact stiffness expressions for the slider in these contact modes through numerical analysis. However, the contact stiffness expression did not consider the lateral contact forces in the contact area between the slider and the guide rail.

Numerous research findings have addressed the study cylindrical pairs, revolute pairs, translational pairs and spherical pairs [14]. The contact areas of the main components of revolute pair and spherical pair are related to the curvature radius of the contacting rigid body, while the contact force resolution for translational pairs requires a more in-depth study of the relative motion of the main components of the translational pair.

The organizational structure of this article is outlined as follows:

In Section 2, a description is provided for common combinations of the slider and the guide rail in 3D translational pair. The joint clearances of the 3D translational pair are classified based on point contact, line contact and surface contact. A total of 11 possible contact forms are summarized. The relative geometric relationship between the center plane of slider and the guide rail is used to derive their respective clearance expressions. Three contact modes for the interaction between the slider and the guide rail are discussed, and a modeling of joint clearances in 3D translational pair is presented, including the derivation of the vector expression of clearances. In Section 3, an analysis is conducted on the contact forces between the slider and the guide rail in 3D translational pair. Addressing the inadequacy of contact stiffness for normal contact forces, the contact areas between the slider and the guide rail are categorized. Mathematical expressions for contact stiffness under different contact areas are derived. Section 4 focuses on the dynamic modeling of the crank slider mechanism, established the dynamic equations for the mechanism. In Section 5, the influence of clearance size, driving speed, and material combination on the dynamics of the crank-slider mechanism is discussed based on motion parameters such as slider displacement, velocity, and acceleration curves, as well as Poincare maps.

2 Translational pair clearance modeling

2.1 Combination of slider and guide rail

In a multibody system, the translational pair provides a degree of freedom for motion along its direction. Typically, translational pairs can be categorized into slider and guide rail combination, pin joint with restricted rotation in a cylindrical groove, and screw nut pairs. Taking the example of the slider and guide rail combination, under ideal conditions, the slider should move linearly along the centerline of the guide rail without experiencing jamming,

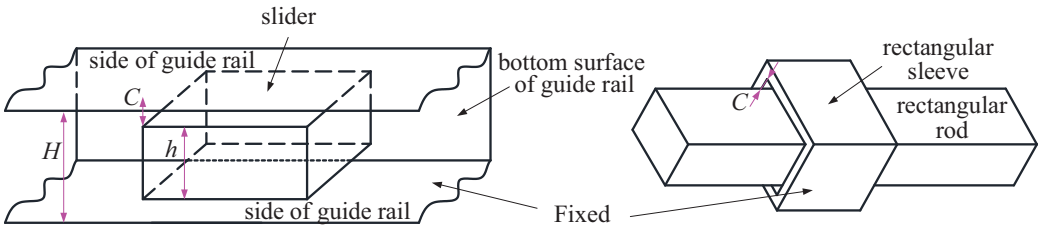

Fig. 1. Two common combinations of 3D translational pairs. (a) The guide rail size is larger than the slider size. (b) The size of the slider is larger than the size of the guide rail.

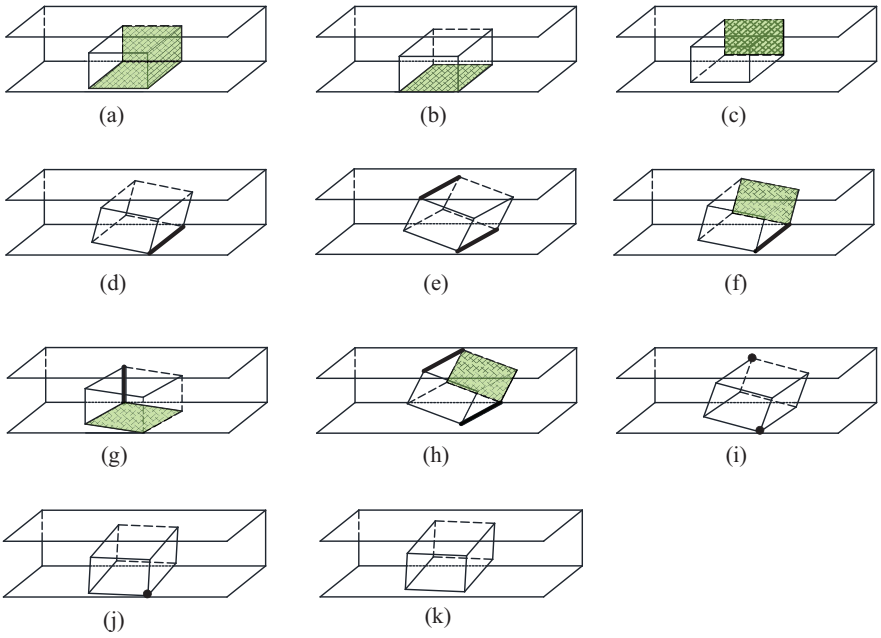

Fig. 2. Possible contact forms between the slide and the guide rail. (a) The form of contact between the side and bottom of the slider and the guide rail. (b) The form of side contact between the slider and the guide rail. (c) The form of contact between the slider and the bottom surface of the guide rail. (d) The form of contact between the slider and a single line of the guide rail. (e) The form of two lines of contact between the slider and the guide rail. (f)–(g) The form of single line contact and bottom contact between the slider and the guide rail. (h) The form of two line contact and bottom contact between the slider and the guide rail. (i) The form of two point contact between the slider and the guide rail. (j) The form of single point contact between the slider and the guide rail. (k) The form of completely noncontact between the slider and the guide rail.

vibration, or motion in other directions. However, in practical industrial applications, translational pairs may exhibit clearances between the slider and guide rail due to machining errors, assembly discrepancies, and material friction and wear. These clearances can impact the motion precision, repeatability and lifespan of mechanical systems. Translational pairs are divided into planar translational pairs and 3D translational pairs. Most research on translational pairs focuses on planar translational pairs [15–17], with limited studied on clearances in 3D translational pairs is. In this section, based on the practical industrial applications of 3D translational pairs, we classify the common combinations of the two main moving components in 3D translational pairs. The classification is illustrated in Figure 1.

Figure 1a depicts the combination of slider and guide rail, while Figure 1b illustrates the combination of rectangular rod within a rectangular sleeve. These two translational pairs are the most common in industrial production. Here, H represents the distance between the two side faces inside the guide rail, h represents the height of the slider, and C represents the clearance between the two main components.

Taking the combination of slider and guide rail as an example, during the motion of the slider along the guide rail, various contact forms can occur between them. By classifying them into point contact, line contact and surface contact, 11 different contact forms can be obtained, as shown in Figure 2.

It is important to note that any of these contact forms may occur, but the probability of all contact forms appearing in a single motion of the translational pair is extremely low. Clearances between the slider and guide rail can introduce errors in the motion of the translational pair. The specific contact form between them depends on the degree of wear and motion characteristics. Considering the diversity of slider motion within the guide rail, the movement forms can be divided into three types.

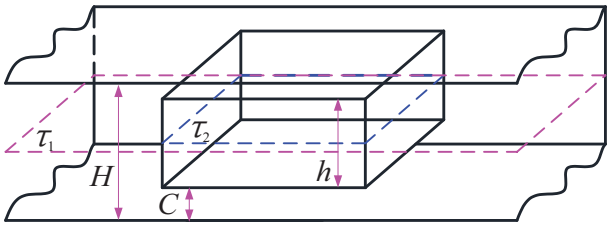

Fig. 3. The center plane of the slider is coplanar with the center plane of the guide rail.

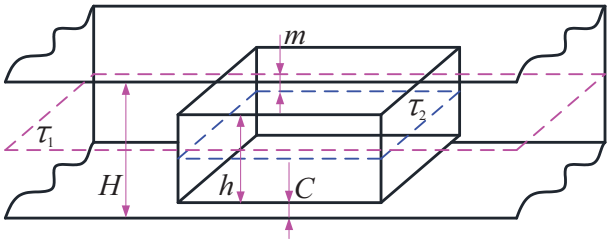

Fig. 4. The center plane of the slider is parallel to the center plane of the guide rail.

The first type is that the center surface of slider coincides with the center surface of guide rail; The second is that the center surface of slider is parallel to the center surface of guide rail, but does not coincide; The third is that the center surface of slider is not parallel to the center surface of guide rail, and the two planes form a certain Angle. The details are shown in Figures 3–5.

Figure 3 depicts the geometric model when the center plane of the slider in the translational pair is coplanar with the center plane of the guide rail.

C represents the distance between the side surfaces of the slider and the guide rail, which can be referred to as the clearance here. H represents the distance between the inner surfaces of the guide rail's two side faces, while h represents the distance between the outer surfaces of the slider's two side faces, τ_1 denotes the center plane of the guide rail, whereas τ_2 corresponds to the center plane of the slider. By considering the geometric relationship depicted in Figure 3, the expression for the clearance can be derived as shown in equation (1):

$$C = \frac{H}{2} - \frac{h}{2}. \tag{1}$$

The geometric model shown in Figure 4 represents a slider and guide rail in the translational pair, where the center plane of the guide rail, denoted as τ_1, and the center plane of the slider, denotes as τ_2, are parallel but not coincident. The distance between these two center planes is represented by m.

The expression for the distance between 2 and its clearance is shown in equation (2):

$$C = \frac{H}{2} - \frac{h}{2} \pm m. \tag{2}$$

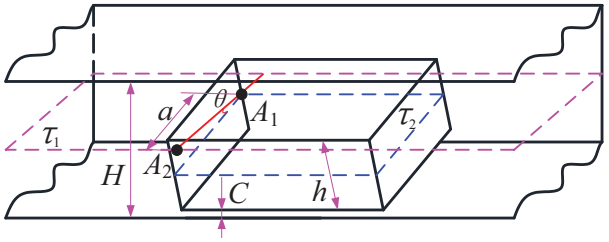

Fig. 5. The center plane of the slider forms a certain angle with the center plane of the guide rail.

Figure 5 shows a geometric model with a certain angle between the center plane of the slider and the center plane of the guide rail.

The module length of A_1A_2 is a. The angle between τ_1 and τ_2 is θ. The clearance expression is shown in equation (3):

$$C = \frac{H}{2} - \frac{h}{2}\cos\theta - a\sin\theta. \tag{3}$$

2.2 Contact conditions between slider and guide rail of translational pair with clearance

As shown in Figure 6, the contact modes between the slider and the guide rail in a translational pair with clearances can be categorized in three types: free flight mode, just contact mode, and pseudo penetration mode.

In the free flight mode, the slider and guide rail do not make any contact, resulting in no contact forces between them. The just contact mode represents a state where the slider and guide rail are in perfect contact without undergoing deformation. The pseudo penetration mode indicates a state where there are force between the slider and the guide rail, and both undergoing deformation. In both the just contact and pseudo penetration modes, contact force are generated, and in pseudo penetration mode, the slider and guide rail may experience varying degrees of deformation. In practice, researchers studying translational pair clearances can determine the mode by assessing the magnitude of the contact forces between them. Specifically, when the contact force between the slider and the guide rail exceeds a certain threshold, the translational joint operates in a pseudo penetration mode. When the contact force between the slider and the guide rail is less than a certain threshold value, the translational joint operates in the free flight mode. When the contact force between the slider and the guide rail is equal to a specific threshold, the translational joint operates in the just contact mode. Therefore, understanding the contact forces between the slider and the guide rail is crucial. However, before analyzing the contact force, it is necessary to first examine the mathematical model of the clearance between the slider and the guide rail.

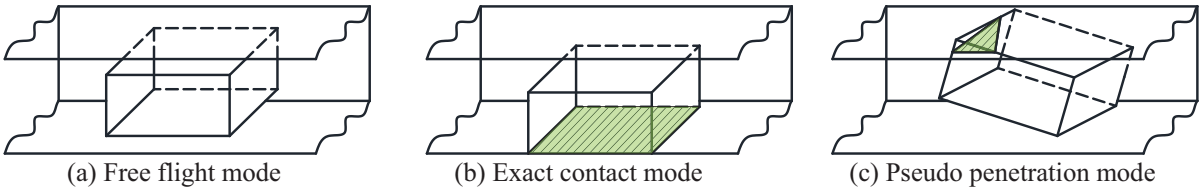

Fig. 6. Three modes of contact between slider and guide rail.

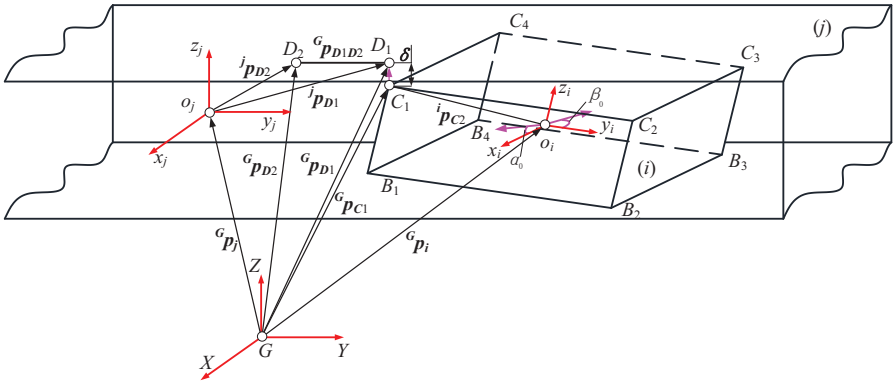

Fig. 7. Modeling of 3D translational pair clearance.

2.3 Modeling of 3D translational pair clearance

In order to better express the geometric relationship between the slider and the guide rail of the translational pair, it is necessary to establish separate local coordinate systems on both the slider and the guide rail. As shown in Figure 7, the slider is represented by i, and the guide rail is represented by j. The center of mass of the slider i is o_i, and the center of mass of the guide rail j is o_j. Establish local coordinate system $\{o_i\}$ and $\{o_j\}$ for the slider and the guide rail, respectively, with their respectively centroids as the origins. In the coordinate system $\{o_i\}$, the x_i axis is parallel to the B_1B_4 direction of the slider, is parallel to the B_1B_2 direction, and the z_i axis is perpendicular to the o_i-x_iy_i plane. In the coordinate system $\{o_j\}$, the y_i axis is parallel to the direction of motion of the slider along the guide rail, the z_j axis is parallel to the cross section of the guide rail, and the x_i axis is perpendicular to the o_j-z_jy_j plane. Here, point C_1 on the slider is considered the closest point to the inner surface of the guide rail, point D_1 on the guide rail is the closest point to the slider. The line C_1D_1 is perpendicular to the side surface of guide rail, and the line D_1D_2 is parallel to the y_j axis of local coordinate system $\{o_j\}$ of the guide rail. The global coordinate system is denoted as $\{G\}$ with axes G-XYZ. α_0 and β_0 represents the roll angle and yaw angle,respectively, of slider i with respect to the global coordinate system $\{G\}$.

Through the geometric relationship between the slider and the guide rail shown in Figure 7, the position vector ${}^{\mathbf{G}}\boldsymbol{p}_{\boldsymbol{C1}}$ expression from the C_1 point on the slider to the global coordinate system $\{G\}$ can be obtained, as shown in equation (4):

$$ {}^Gp_{C1} = {}^Gp_i + R_i\,{}^ip_{C1}. \tag{4} $$

In equation (4), ${}^{\boldsymbol{G}}\boldsymbol{p}_{\boldsymbol{i}}$ represents the position vector from the origin of the local coordinate system $\{o_i\}$ to the origin of the global coordinate system $\{G\}$. R_i is the rotation matrix from the local coordinate system $\{o_i\}$ to the global coordinate system $\{G\}$, and ${}^{\boldsymbol{i}}\boldsymbol{p}_{\boldsymbol{C1}}$ is the position vector of the point C_1 relative to the local coordinate system $\{o_i\}$. To describe the position vector of point D_1 on the guide rail relative to the global coordinate system $\{G\}$, we define a unit vector s_j in the direction from point D_2 to point D_1. The expression for this vector is given by equation (5):

$$ s_j = \frac{R_j({}^jp_{D2} - {}^jp_{D1})}{\|R_j({}^jp_{D2} - {}^jp_{D1})\|}. \tag{5} $$

In equation (5), R_j represents the rotation matrix from the local coordinate system $\{o_j\}$ of the guide rail to the global coordinate system $\{G\}$. ${}^{\boldsymbol{j}}\boldsymbol{p}_{\boldsymbol{D2}}$ is the position vector of point D_2 in the local coordinate system $\{o_j\}$, and ${}^{\boldsymbol{j}}\boldsymbol{p}_{\boldsymbol{D1}}$ is the position vector of point D_1 in the local coordinate system $\{o_j\}$. The vector expression for the displacement from point D_2 to point D_1 relative to the global coordinate system $\{G\}$ is given by equation (6):

$$ {}^Gp_{D2D1} = s_j^T({}^Gp_{D2} - {}^Gp_{C1})s_j. \tag{6} $$

According to the geometric relationship between the vectors shown in Figure 7, it is easy to obtain the position vector of point D_1 on the global coordinate system $\{G\}$, as shown in equation (7):

$$ {}^Gp_{D1} = {}^Gp_{D2} + {}^Gp_{D2D1}. \tag{7} $$

Substituting equation (6) into equation (7) yields equation (8):

$$^{G}p_{D1} = {}^{G}p_{D2} + s_j^T({}^{G}p_{D2} - {}^{G}p_{C1})s_j. \tag{8}$$

The distance between the slider and the closest point on the guide rail, which is point C_1, can be easily expressed mathematically as the clearance δ. The relationship can be derived from vector analysis, and it is given by equation (9):

$$\delta = {}^{G}p_{D1} - {}^{G}p_{C1}. \tag{9}$$

Next, the contact status between the slider and the guide rail is analyzed using the expression for the clearance. When the slider and guide rail in the translational pair are in free flight mode, they are not in contact. This situation can be mathematically represented by equation (10):

$$s_j^T \delta > 0. \tag{10}$$

When the slider and guide rail are in just contact mode and pseudo penetration mode, the mathematical expression is shown in equation (11):

$$s_j^T \delta \leq 0. \tag{11}$$

By taking the derivative of equation (9), the relative contact velocity between the slider and the guide rail can be obtained, as shown in equation (12):

$$\dot{\delta} = G\dot{p}_D - G\dot{p}_B. \tag{12}$$

Due to the nonlinear movement characteristics of the slider in the guide rail groove, accurately describing the dynamic characteristics of the slider while moving in the guide rail requires decomposing its relative contact velocity into tangential and normal components. The specific expression for these components are given by equation (13):

$$\begin{cases} v_n = (\dot{\delta})s_j^T \\ v_t = (\dot{\delta})s_j \end{cases}. \tag{13}$$

Based on the tangential and normal velocities in equation (13), the motion trend between the slider and the guide rail can be determined. By assessing the observed motion trend, the contact status between the slider and guide rail can be further evaluated.

3 Analysis of contact force model

In an ideal scenario, the slider and guide rail experience smooth and linear motion without any clearances. However, the existence of the clearance in practical translational pair leads to changes in the motion process. Problems like collisions, wear between the slider and the guide rail emerge, affecting the motion accuracy, transmission efficiency, and lifespan of the translational pair [18]. The contact forces generated during the collision or wear processes between them play a crucial role in the overall motion performance of the translational pair. Therefore, this section models the contact forces generated between the slider and the guide rail. Contact forces can be decomposed into normal forces and tangential forces based on the contact area between the slider and the guide rail. Next, it is necessary to analyze the normal forces and tangential forces.

3.1 Normal contact force model

Translational pairs with clearances generate heat during the motion process, and this heat is considered part of the initial energy of the translational pair. It leads to a reduction in the transmission efficiency of the translational pair. In other words, if the guide rail remains stationary, the actual kinetic energy of the slider will decrease [19]. In the study of contact forces with energy loss, among various models proposed by scholars, the model presented by Hunt and Crossley [20] is the most representative, as shown in equation (14):

$$\boldsymbol{F}_n = k\delta^n + b\delta^p\dot{\delta}^q. \tag{14}$$

Equation (14) consists of elastic force term and damping term. The part after the plus sign belongs to the damping term, where δ is the relative deformation between the slider and guide rail, b represents the damping coefficient, n indicates the material stiffness exponent, which is an intrinsic property of the material. p is determined by the deformation of the slider and guide rail, and q is determined by their impact velocity. The contact stiffness coefficient k is determined by the material properties and physical parameters of the slider and guide rail, and its expression is shown in equation (15) [11]:

$$k = \frac{4}{3\pi(\sigma_i + \sigma_j)} R^{1/2}. \tag{15}$$

where [11],

$$\sigma_l = \frac{1 - \nu_l^2}{\pi E_l} (l = i, j). \tag{16}$$

$$R = \frac{R_i R_j}{R_i \pm R_j}. \tag{17}$$

In equation (15), R represents the curvature radius of two contacting objects. Here, it is assumed that the surfaces of both contacting objects are spherical. R_i and R_j are the radii of two objects in contact with each other. The parameters σ_i and σ_j are determined by equation (16), while R is calculated using equation (17). In equation (16), E_l and ν_l represent the Young's modulus and Poisson's ratio of the contact material, respectively. If the contacting surfaces of two objects are planar, equation (14) only includes the elastic force term, and the damping term is no longer exists. Therefore, equation (14) undergoes a

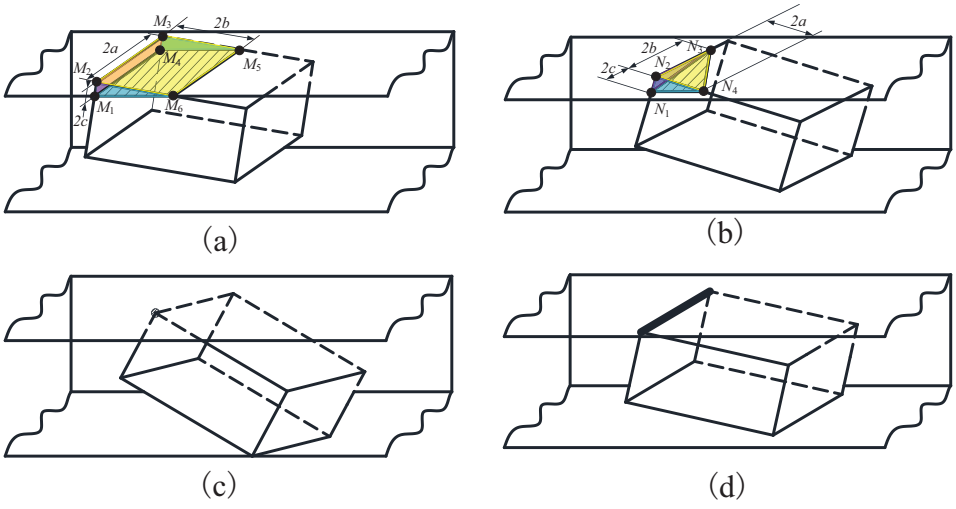

Fig. 8. Classification of the contact area between the slider and the guide rail. (a) The situation when the contact area are rectangular and triangular. (b) The situation when the contact area are triangular. (c) The situation when the contact is a point contact. (d) The situation when the contact is line contact.

modification, as shown in equation (18):

$$\boldsymbol{F}_n = k\delta^n. \tag{18}$$

In equation (18), the contact force is linear because the contacting objects do not possess an inherent curvature, making it a reasonable assumption. In this case, since both the slider and the guide rail do not have curvature radius, their contact is not analogous to two spheres touching each other. Therefore, the formula for the contact stiffness coefficient k also undergoes changes based on the physical dimensions of the contacting object, as shown in equation (19) [11]:

$$k = \frac{d}{0.475(\sigma_i + \sigma_j)}. \tag{19}$$

In equation (19), $2d$ represents the side length of the contact area between two objects, assuming the contact area to be a square by default. However, it is not always the case that the contact area between slider and guide rail remains a square without undergoing any changes. When the contact area described in equation (19) is no longer applicable. Depending on the geometric dimensions of the slider and guide rail, there are four possible scenarios when a collision occurs, categorized based on the geometric shape of the contact area: rectangular, triangular, point, and line, as illustrated in Figure 8

Figure 8a depicts the case where the contact area between the slider and guide rail is a rectangular region. From Figure 8a, it can be observed that there are four contact surface between the slider and guide rail: surfaces $M_1M_2M_6$, face $M_3M_4M_5$, face $M_1M_2M_3M_4$, and face $M_2M_3M_5M_6$. When the contact area is rectangular, the bottom surface of the slider and the bottom surface of the guide rail are parallel. Therefore, the contact force generated by surfaces $M_1M_2M_6$ and $M_3M_4M_5$ should be parallel to the side surface of either the slider or guide rail, with equal magnitude and opposite directions. Hence, it is unnecessary to consider the magnitudes of the contact forces from these two surfaces. With respect to the side surface of the guide rail, the normal contact forces generated by surfaces $M_1M_2M_3M_4$ and $M_2M_3M_5M_6$ should have a projection area on the guide rail side surfaces $M_1M_4M_5M_6$. The magnitude of the contact stiffness k for the contact area represented by surface $M_2M_3M_5M_6$ has been concluded in reference [13], and its stiffness expression is given in equation (20):

$$k_{M_2M_3M_5M_6} = \frac{\sqrt{S_{M_2M_3M_5M_6}}}{\sigma_i + \sigma_j} \frac{1}{11.15\left(\frac{a}{b} + 15.72\right)^{-1} + 0.2854}. \tag{20}$$

In equation (20), $S_{M2M3M5M6}$ represents the area size of the face $M_2M_3M_5M_6$, and $2a$ and $2b$ represent the length and width of the rectangular face. Due to the fact that both faces $M_1M_2M_3M_4$ and $M_2M_3M_5M_6$ are rectangular, the same calculation method can be used to easily determine the magnitude of the contact stiffness possessed by face $M_1M_2M_3M_4$, as shown in equation (21):

$$k_{M_1M_2M_3M_4} = \frac{\sqrt{S_{M_1M_2M_3M_4}}}{\sigma_i + \sigma_j} \frac{1}{11.15\left(\frac{a}{c} + 15.72\right)^{-1} + 0.2854}. \tag{21}$$

Figure 8b illustrates the case where the contact area between the slider and guide rail is a triangular region. From Figure 8b, it can be observed that there are three triangular contact surfaces between the slider and guide rail, namely $N_1N_2N_4'$face $N_1N_2N_3$ and $N_2N_3N_4$. The size of these three triangular surfaces are determined by the deflection angle of the slider relative to the guide rail. The expressions for the contact stiffness of these three contact

surfaces are given in equation (22):

$$\begin{cases} k_{N_2N_3N_4} = \dfrac{\sqrt{S_{\Delta N_2N_3N_4}}}{\sigma_i+\sigma_j}\dfrac{1}{9.924\left(\dfrac{a}{b}+14.70\right)^{-1}+0.2731} \\ k_{N_1N_2N_4} = \dfrac{\sqrt{S_{\Delta N_1N_2N_4}}}{\sigma_i+\sigma_j}\dfrac{1}{9.924\left(\dfrac{a}{c}+14.70\right)^{-1}+0.2731} \\ k_{N_1N_2N_3} = \dfrac{\sqrt{S_{\Delta N_1N_2N_3}}}{\sigma_i+\sigma_j}\dfrac{1}{9.924\left(\dfrac{b}{c}+14.70\right)^{-1}+0.2731)} \end{cases}. \tag{22}$$

Figure 8c represents the scenario where the slider and the guide rail make point contact. In this case, point contact can be considered as the contact between a small spherical surface and plane. Figure 8d illustrates the scenario where the slider and guide rail make line contact. In this case, it can be considered as the contact between a small cylinder surface with a small radius and a plane. The normal contact forces generated in both of these cases can be expressed using equation (23):

$$\boldsymbol{F}_n = k\delta^{3/2} + b\dot{\delta}. \tag{23}$$

The stiffness parameter k in equation (23) can be calculated using equation (15), and the damping coefficient b is expressed as equation (24):

$$b = \frac{3k(1-c_e^2)\delta^n}{4\dot{\delta}^{(-)}}. \tag{24}$$

In equation (24), c_e represents the coefficient of restitution, which is the ratio of the relative velocity of the slider and guide rail after impact to the previous one. $\dot{\delta}^{(-)}$.represents the normal initial velocity when the slider and guide rail come into contact.

3.2 Tangential contact force model

When the slider and guide rail come into contact, they generate normal contact forces perpendicular to the contact surface and tangential contact forces parallel to the contact surface. Next, the tangential contact forces will be described using Coulomb's friction law [21,22]. According to Coulomb friction theory, the coefficient of friction is determined by the material properties of the slider and guide rail. As the relative velocity and magnitude of the load between the slider and guide rail change, the friction coefficient also undergoes continuous variations. In the context, this paper refers to the changing friction coefficient as the generalized friction coefficient, denoted by the symbol $\mu\ (v_t)$. According to the modified Coulomb's friction law discussed in reference [23], the expression for tangential contact force can be obtained equation (25):

$$\boldsymbol{F}_t = -\mu(v_t)F_n sgn(v_t). \tag{25}$$

In equation (25), F_n represents the normal contact force, sgn (v_t) is the sign function of the tangential velocity v_t, and the generalized friction coefficient $\mu\ (v_t)$ is also a function of tangential velocity v_t, and its expression is shown in equation (26):

$$\mu(v_t) = \begin{cases} 0 & \text{for } |v_t| \le v_0 \\ \mu_d \dfrac{|v_t|-v_0}{v_1-v_0} & \text{for } v_0 \le |v_t| \le v_1 \\ 1 & \text{for } |v_t| \ge v_1 \end{cases}. \tag{26}$$

In equation (26), v_0 and v_1 are the range of tangential velocities, μ_d is the dynamic friction coefficient related to the collision material.

Next, an analysis will be conducted on the effects of variable stiffness and constant stiffness on the contact force between the slider and guide rail. The inclination of the slider within the guide rail is determined by the roll angle α_0 and yaw angle β_0 as shown in Figure 7. By combining equations (19)–(22), the contact force variation curves between the slider and guide rail can be derived under both variable stiffness and constant stiffness, as illustrated in Figure 9. It is assumed in Figure 9 that the initial contact velocity between the slider and guide rail is both 1 m/s.

Figures 9(a–9d) shows the variation trend of the contact force between the slider and the guide rail when $\alpha_0 = 0°$, $\beta_0 = 0.3°$, $\alpha_0 = 0°$, $\beta_0 = 1.5°$, $\alpha_0 = 0.3°$, $\beta_0 = 1.5°$ and $\alpha_0 = 1.5°$, $\beta_0 = 1.5°$, respectively. Figures 9a and b shows that the slider only generates yaw relative to the guide rail and does not roll over. As shown in Figures 9c and 9d, the slider simultaneously yaws and rolls relative to the guide rail. The figure shown in Figure 9e illustrates the variation of contact stiffness with different poses of the slider. In the four states shown in Figure 9, the contact force peaks obtained by the variable stiffness model are all smaller than those under the constant stiffness model, and the continuous contact time is slightly longer.

4 Dynamic model of 3D crank slider mechanism with clearance between translational pair

Figure 10 illustrates a typical 3D model of a crank slider mechanism, which consists of only revolute pairs, translational pair and spherical pair. This section defaults to revolute pairs and spherical pair being perfect, with no clearances in the kinematic pairs. Only the translational pair has clearances, and its motion can be classified into three modes: free flight mode, just contact mode, and pseudo penetration mode.

The crank slider mechanism consists of three moving rigid bodies: the crank, the connecting rod, and the slider. $\boldsymbol{q}$ represents the generalized coordinate vector of the multi-body system, and it can be expressed in terms of the centroid coordinates (x, y, z) and the orientations $(\alpha'\beta'\gamma)$ of these three moving rigid bodies, as shown in equation (27):

$$\boldsymbol{q}_i = [x, y, z, \alpha, \beta, \gamma]^T, \boldsymbol{q} = [\boldsymbol{q}_1, \boldsymbol{q}_2, \ldots, \boldsymbol{q}_n]. \tag{27}$$

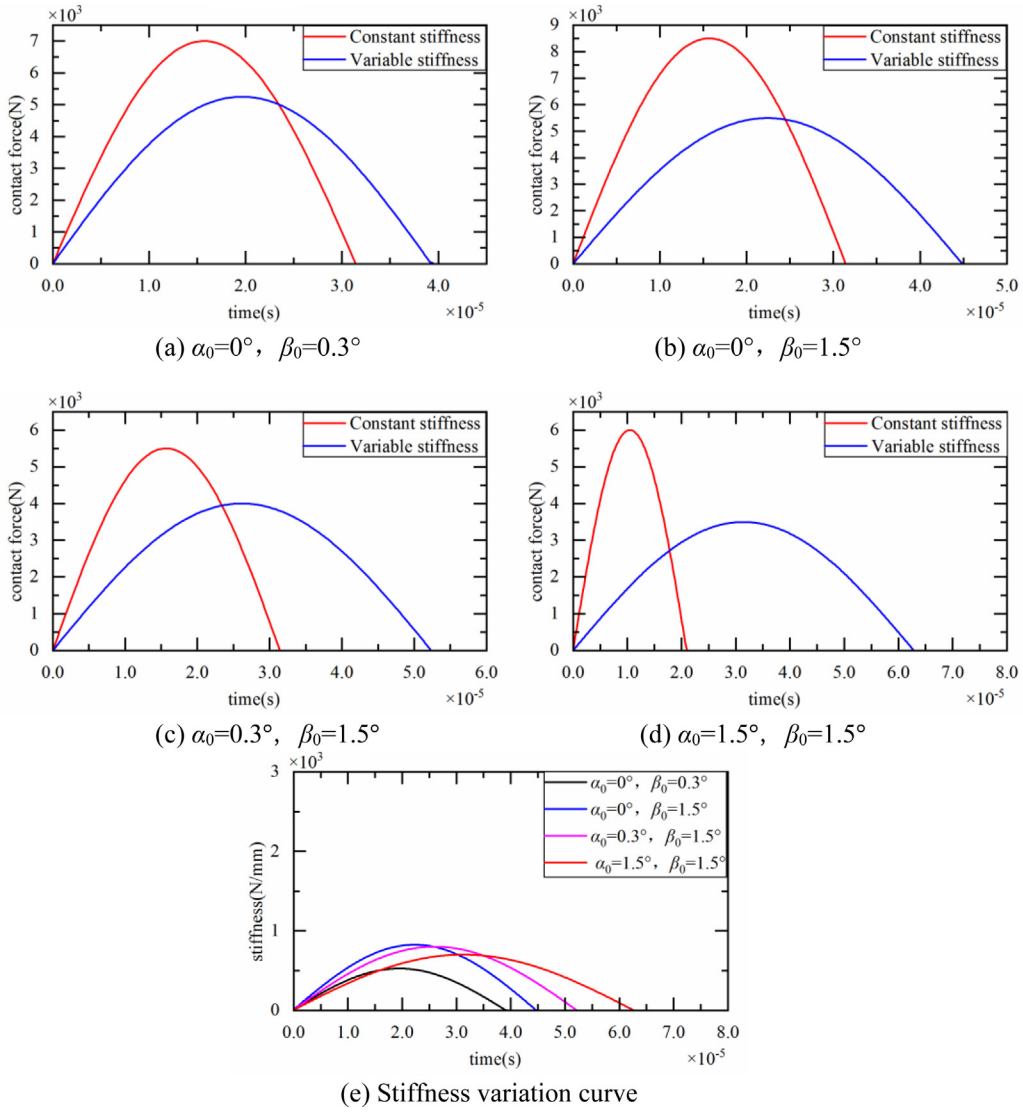

Fig. 9. Comparison curve between variable stiffness model and constant stiffness model.

n denotes the number of active components in a multibody system, and the constraint equation system of the crank slider mechanism is equation (28):

$$\phi^K(\boldsymbol{q}) = [\phi_1^K(\boldsymbol{q}), \phi_2^K(\boldsymbol{q}), \ldots, \phi_n^K(\boldsymbol{q})]. \tag{28}$$

The revolute pair located at the connection between the crank and the frame provides the driving force for the multibody system. If this driving pair is constrained, the multibody system cannot move. Therefore, the constraint for this driving is expressed as equation (29):

$$\phi^D(\boldsymbol{q}, t) = 0. \tag{29}$$

By combining equation (28) and equation (29), all constraint equation (30) of the multibody system can be obtained:

$$\phi(\boldsymbol{q}, t) = \begin{bmatrix} \phi^K(\boldsymbol{q}, t) \\ \phi^D(\boldsymbol{q}, t) \end{bmatrix} = 0. \tag{30}$$

According to the Lagrange multiplier method, the dynamic equation of the crank slider mechanism with clearance can be obtained as shown in equation (31):

$$\begin{cases} M(q)\,\ddot{q} + C(q,q)\dot{q} + Q(\dot{q}) + G(q) = F(t) + F_C(t) \\ \phi(q,t) = 0 \end{cases}. \tag{31}$$

The expression of $\boldsymbol{F}_C(t)$ in the table is shown in equation (32):

$$\boldsymbol{F}_C(\boldsymbol{t}) = u(\delta)(\boldsymbol{F}_n + \boldsymbol{F}_t). \tag{32}$$

In equation (32), $u(\delta)$ is the step function about δ, as shown in equation (33):

$$u(\delta) = \begin{cases} 0 & \delta < 0 \\ 1 & \delta \geq 0 \end{cases}. \tag{33}$$

The specific meanings of $\boldsymbol{M}(\boldsymbol{q})'\boldsymbol{q}'\,C(q,q).'\,Q(\dot{q}).'\boldsymbol{G}(\boldsymbol{q})'\boldsymbol{F}(t)'\boldsymbol{F}_{\boldsymbol{C}}(t)$are shown in Table 1:

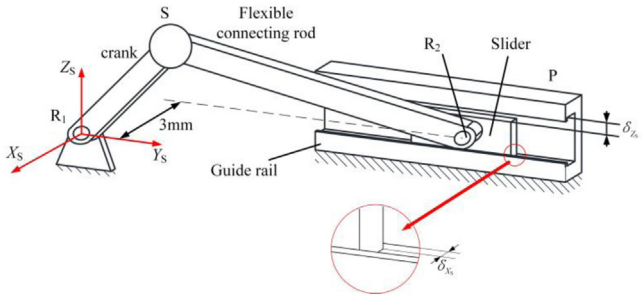

Fig 10. 3D model of crank slider mechanism.

5 Simulation results and discussion

In this section, the effect of joint clearances in the crank slider mechanism on the motion of the slider and crank is studied. The geometric dimensions and mass properties of the active components (crank, connecting rod, slider) in the mechanism are listed in Table 2. The material properties of the mechanism are described in Table 3. The materials of the crankshaft, connecting rod, and slider are all aluminum alloy materials.

Next, the main factors influencing the motion characteristics of a 3D crank-slider mechanism will be discussed by comparing different clearances, different driving speeds, and different material combinations between the slider and the guide rail.

5.1 Influence of different clearances on the motion characteristics of the 3D crank slider mechanism

In the 3D crank slider mechanism shown in Figure 10, only the translational pair has clearances in two directions, while the other kinematic pairs are ideal joints without clearances. The crank drives the slider in the guide rail through an electric motor, with a driving speed of 20 rpm. The materials of the slider and the guide rail in the translational pair are both alloy steel, respectively. The clearances in the X_S and Z_S directions of the translational pair are set to 0.1 mm and 0.5 mm, respectively, for motion simulation.

Figure 11 shows the displacement change of the slider under different clearances, with a local magnified view. It can be seen from Figure 11 that when the clearances in the X_S and Z_S directions of the translational pair are 0.1 mm, the influence on the slider displacement is small, with slight fluctuations in displacement as shown in the local magnified view. However, when the clearance increases to 0.5 mm, the fluctuation in slider displacement caused by the clearance begins to increase, with more obvious fluctuations at the peaks and valleys of the displacement.

Figure 12 shows the overall fluctuation curve of the slider acceleration under different clearances, with a local magnified view of the slider acceleration. It can be seen from both figures that the size of the clearance in the translational pair has a significant impact on the slider acceleration. Generally, as the clearance value increases, the influence of the clearance on the fluctuation of the slider acceleration also increases. When the clearance is 0.1 mm, the maximum fluctuation amplitude of the acceleration is 190.8 mm/s^2 at 4.26 s, which is 1.5 times the theoretical value of the acceleration at that point. When the clearance is 0.5 mm, the influence of the clearance on the slider acceleration is significant throughout the acceleration curve. At the peaks and valleys of the acceleration curve, the maximum fluctuation amplitude of the acceleration caused by the clearance can reach 413.3 mm/s^2 at 4.95 s, which is 3.4 times the theoretical value of the acceleration at that point.

5.2 Influence of different driving speeds on the motion characteristics of 3D crank slider mechanism

To better analyze the influence of different driving speeds on the motion characteristics of the mechanism with clearance, it is assumed that the clearance of the translational pair in the Z_S and Y_S directions remains at 0.1 mm. The materials of the slider and the guide rail in the translational pair are aluminum alloy and alloy steel, respectively. The driving speeds of the crank are set to 20, 50, 100, and 180 rpm, respectively. This section only analyzes the trend of the slider's acceleration.

Figure 13 shows the acceleration curves of the slider under different driving speeds. It can be seen from the four graphs in Figure 13 that the driving speed has a greater influence on the slider's acceleration. Taking the speeds of 20 rpm and 180 rpm as examples, when the speed is 20 rpm, the maximum fluctuation amplitude of the slider's acceleration is 190.92 mm/s^2, which is 1.5 times the theoretical acceleration at the same time point. When the speed is 180 rpm, the maximum fluctuation amplitude of the acceleration is 23.79 m/s^2, which is 2.4 times the theoretical acceleration at the same time point. This shows that the higher the speed, the greater the fluctuation in the slider's acceleration.

5.3 Influence of different material combinations in the translational pair on the motion characteristics of the 3D crank slider mechanism

This section aims to discuss the influence of different material combinations between the slider and the guide rail in the translational pair on the motion characteristics of the 3D crank slider mechanism. The guide rail material of the translational pair is set to aluminum alloy, and the slider materials are alloy steel, nodular cast iron, copper alloy, and aluminum alloy, respectively. The driving speed is 20 rpm, and the clearances in the X_S and Z_S directions of the translational pair are 0.1 mm. Factors such as deformation and wear are not considered in the simulation process. The material parameters are shown in Table 4, and the friction coefficients for the material combinations are shown in Table 5.

Figure 14 show the displacement curves of the slider under different material combinations between the slider and the guide rail, respectively, with their respective local magnified views. It can be seen from Figure 14 that the influence of different material combinations in the

Table 1. Parameter meanings of dynamic equations.

$M(q)$	Mass matrix of the entire multi body system of the crank slider mechanism
$\boldsymbol{q}$	Generalized coordinate vector
$C(q.q)$	Coriolis force matrix
$Q(\dot{q})$	Friction torque
$\boldsymbol{G}(\boldsymbol{q})$	Gravity matrix
$\boldsymbol{F_C}(t)$	Constraints of translational pair with clearances
$\boldsymbol{F}(t)$	Generalized force matrix

Table 2. The geometric dimensions and quality attributes of crank slider mechanism.

Parts	Length (mm)	Mass (kg)	Characteristics of inertia (kg m^2)					
			J_{xx}	J_{yy}	J_{zz}	J_{xy}	J_{xz}	J_{yz}
Crank	40	0.024	8.433×10^{-5}	8.638×10^{-5}	1.366×10^{-5}	3.480×10^{-6}	1.158×10^{-5}	1.944×10^{-5}
Flexible Connecting rod	130	0.075	5.439×10^{-4}	5.514×10^{-4}	1.247×10^{-5}	3.729×10^{-6}	5.593×10^{-5}	2.797×10^{-5}
Slider	–	0.019	7.340×10^{-5}	6.198×10^{-5}	5.541×10^{-6}	3.943×10^{-6}	1.948×10^{-6}	1.399×10^{-5}

Table 3. Parameters used in the dynamic simulation of the crank slider mechanism.

Parameter	Value
Coefficient of friction	0.17
Coefficient of restitution	0.58
Young's modulus	72GPa
Poisson's ratio	0.37
Integration step size	1×10^{-3}s
Integration tolerance	1×10^{-7}

translational pair on the slider's displacement is relatively small, and the fluctuations in displacement shown in the local magnified views are also small.

Figure 15 shows the acceleration curves of the slider under different material combinations between the slider and the guide rail, with their respective local magnified views. From Figure 15a, it can be seen that when the slider and the guide rail have different material combinations in the translational pair, the overall trend of the slider's acceleration curve remains consistent. However, as shown in the local magnified view in Figure 15b, when the slider and the guide rail are composed of aluminum–aluminum combination, the amplitude of the acceleration fluctuation at the peaks and valleys of the acceleration curve is slightly larger than that of other material combinations.

5.4 Research on chaos phenomenon of 3D crank slider mechanism during moving clearance

The clearance of the kinematic pair intensifies the nonlinear motion of the multibody mechanical system, thereby inducing chaotic behavior within the system. Consequently, this study investigates the effects of clearance size, driving speed, and material combination on system chaos in light of their aforementioned influences on the dynamic characteristics of the crank slider mechanism.

(1) The influence of clearances on chaotic phenomena

Assuming that the clearance values in the X_S and Z_S directions of the translational pair are the same, with clearance values of 0.1 mm and 0.5 mm, and the crank speed is 50 rpm. The material of the guide rail and slider is aluminum alloy. The strength of the chaotic phenomenon in the system is determined by studying the relative displacement and relative velocity of the slider's center of mass in the X_S direction with the Poincare section's intersection status.

Figure 16 shows the relative displacement and velocity of the slider's center of mass in the X_S direction under different clearances. Observing Figure 16, it can be seen that the mapping points of the slider's center of mass in the X_S direction and velocity on the Poincare section are clustered, nonclosed, and exhibit certain regularity. Comparing the concentration of mapping points in each graph reveals that as the clearance size of the translational pair increases, the chaotic phenomenon in the system becomes stronger.

(2) The influence of driving speed on chaotic phenomena

With a clearance size of 0.5 mm, and crank speeds of 50, 100, 200, and 500 rpm, without considering factors such as wear and deformation in the kinematic pair clearance, only the effect of driving speed on the chaotic phenomenon of the crank-slider mechanism is studied. The material of the guide rail and slider is aluminum alloy. Figure 17 shows the relative displacement of the slider's center of mass in the X_S and Z_S directions under different driving speeds.

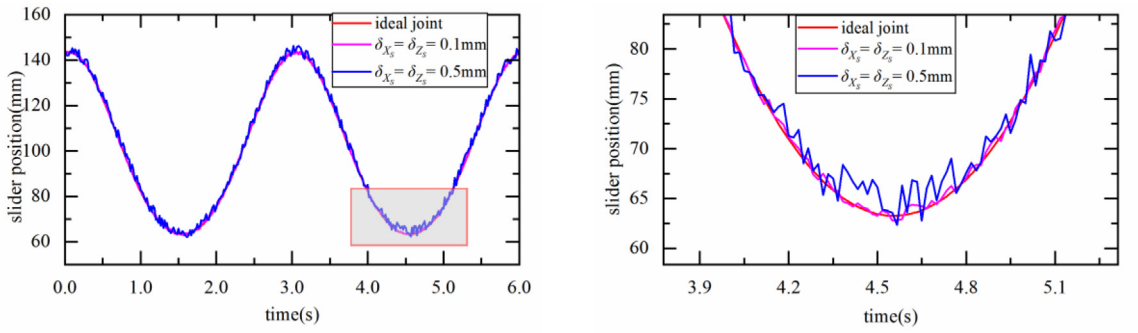

(a) The displacement curve of the slider (b) Local magnified view of slider displacement

Fig. 11. Slider displacement and local magnified view of translational pair with different clearances in X_S and Z_S directions.

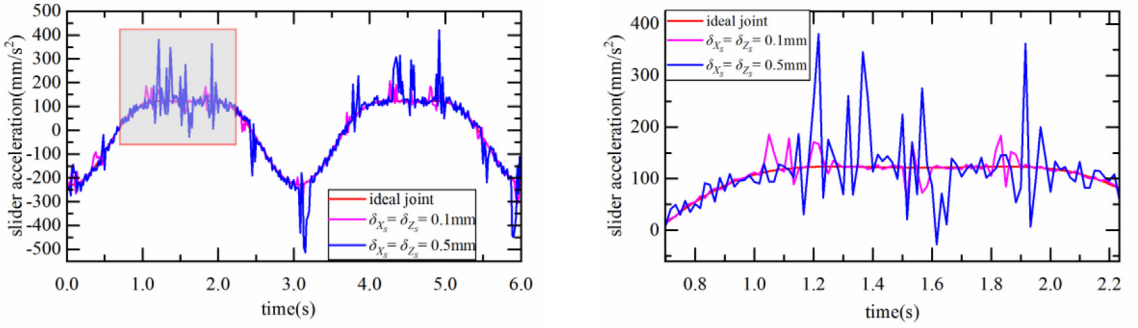

(a) The acceleration curve of the slider (b) Local magnified view of slider acceleration

Fig. 12. Slider acceleration and local magnified view of translational pair with different clearances in X_S and Z_S directions.

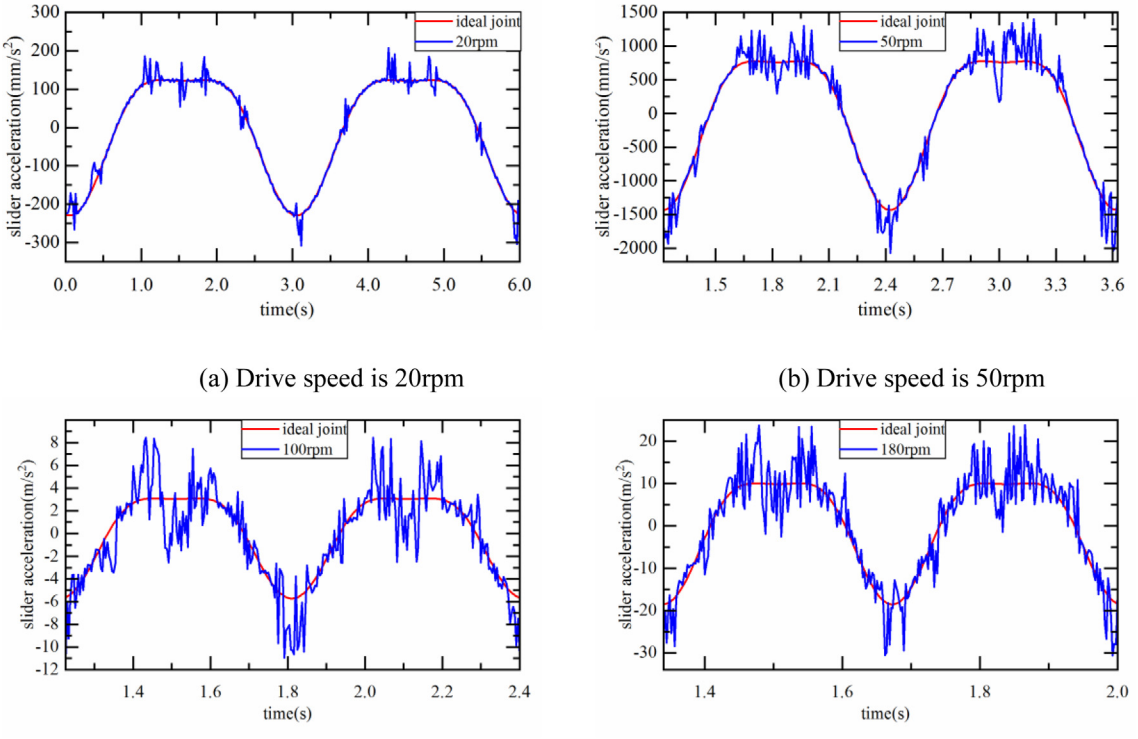

(a) Drive speed is 20rpm (b) Drive speed is 50rpm

(c) Drive speed is 100rpm (d) Drive speed is 180rpm

Fig. 13. The acceleration curves of the slider under different driving speeds.

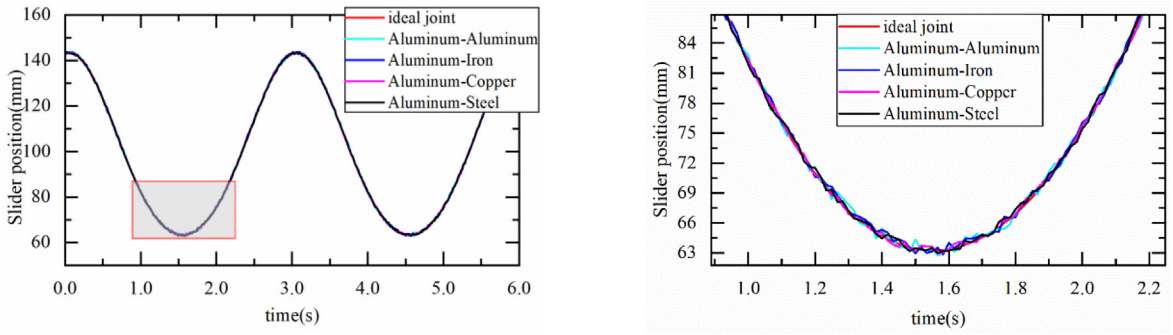

(a) Displacement curve of slider under different material combinations (b) Local magnified view

Fig. 14. Slider displacement under different material combinations of slider and guide rail.

Table 4. Parameters of each material.

Material	Young's modulus (GPa)	Poisson's ratio	Density (kg/m^3)
Steel	207	0.29	7801
Nodular cast iron	173	0.3	7300
Copper	106	0.324	8545
Aluminium	72	0.33	2750

Table 5. Friction coefficient during dry friction between materials.

Friction coefficient	Aluminium – Steel	Aluminium – Copper	Aluminium – Iron	Aluminium – Aluminium
Static friction	0.61	0.6	0.49	0.25
Kinetic friction	0.47	0.46	0.31	0.14

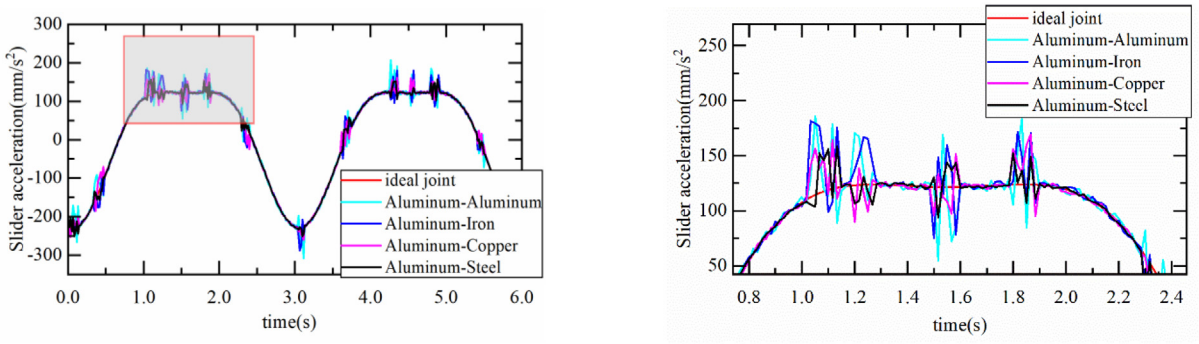

(a) Acceleration curve of slider under different material combinations (b) Local magnified view

Fig. 15. The acceleration curves of the slider under different material combinations between the slider and the guide rail.

From Figure 17a, it can be seen that when the driving speed is 50 rpm, the mapping points of the slider's center of mass in the X_S and Z_S directions on the Poincare section are scattered and exhibit a very obvious chaotic phenomenon. From Figure 17d, it can be seen that when the driving speed is 500 rpm, the mapping points in the Poincare map are not completely closed, but the distribution of these mapping points is very regular. According to the Poincare mapping judgment criterion, there are a few discrete points in the Poincare mapping, indicating that the system changes from chaotic motion to periodic motion. It can be seen that as the driving speed increases, the chaotic phenomenon in the system gradually weakens.

(3) The influence of different material combinations on chaotic phenomena

Selecting aluminum alloy as the guide rail material for the translational pair and the slider materials successively as aluminum alloy, nodular cast iron, copper alloy, and

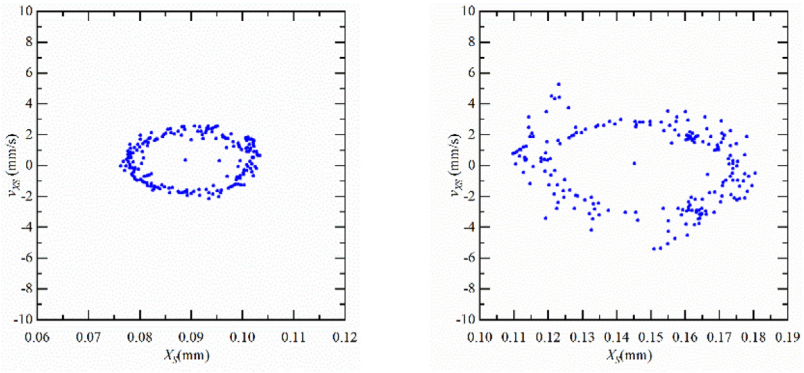

Fig. 16. Poincare mapping diagram of mechanisms under different clearances.

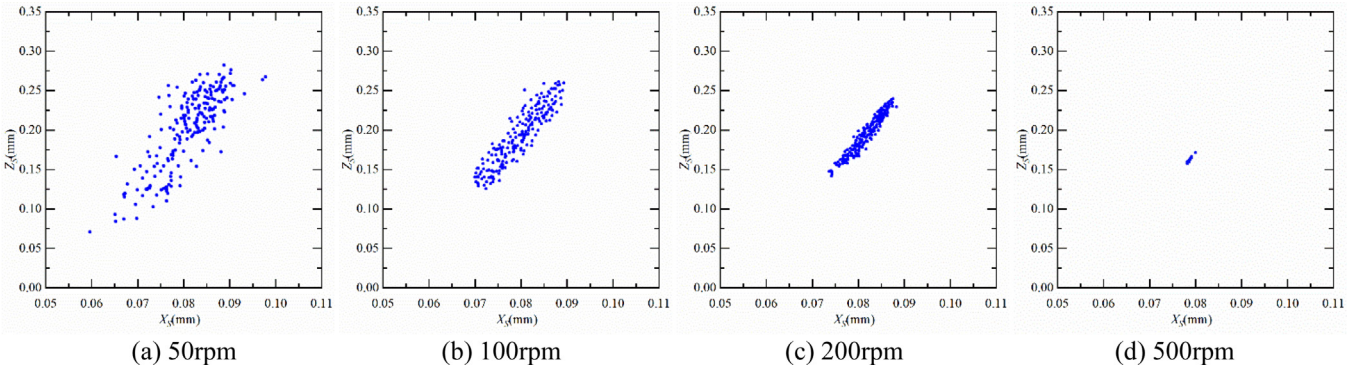

Fig. 17. Poincare mapping diagram of mechanisms under different driving speeds.

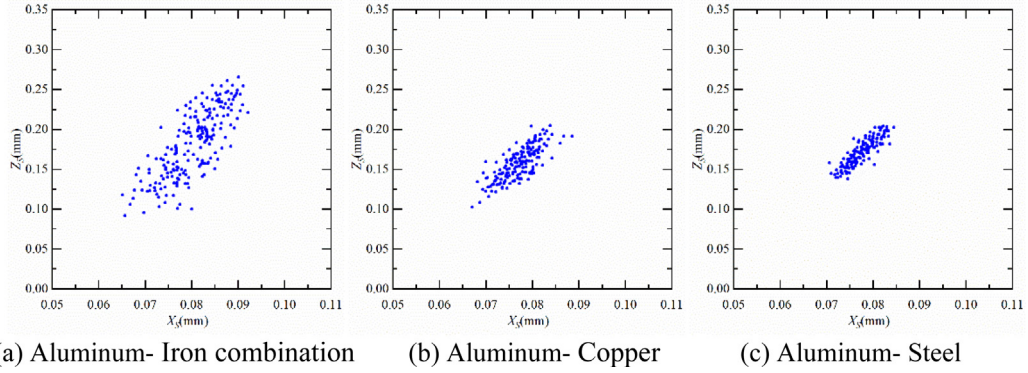

Fig. 18. Poincare mapping diagram of mechanisms under different material combinations.

alloy steel, the influence of different material combinations in the translational pair on the chaotic phenomenon of the system is analyzed. With a clearance of 0.5 mm and a crank speed of 50 rpm, since Figure 17a shows the relative displacement of the slider's center of mass in the X_S direction and Z_S direction for the aluminum-aluminum combination, only Poincare maps for the other three material combinations are plotted, as shown in Figure 18.

When the guide rail and slider materials are aluminum-steel combination, the system exhibits the weakest chaotic motion, and when they are aluminum-aluminum combination, the system exhibits the strongest chaotic motion. Since the friction coefficients of the aluminum-steel combination and the aluminum-copper combination are very close, the distribution of the intersection points between the slider's center of mass in the X_S direction and Z_S direction and the Poincare section is also closest in these two combinations. It can be concluded that the chaotic motion of the system decreases as the friction coefficient between the slider and the guide rail increases.

6 Conclusions

This article takes the crank slider mechanism as the research object, in which only the translational pair has joint clearance, in order to study the dynamic characteristics of the 3D crank slider mechanism when there are joint clearances in the 3D translational pair.

Firstly, the 11 possible contact forms between the slider and the guide rail of the 3D translational pair are summarized. It is noted that any of the above contact forms may occur, but the probability of all contact forms occurring in a single translation pair is very small. Secondly, based on the geometric characteristics of the contact area between the slider and the guide rail, both the frontal contact and the lateral contact of the contact area are considered. The mathematical expressions for the contact stiffness in different contact areas are derived, and a contact force model between the slider and the guide rail is established to simulate and analyze the dynamics of the crank-slider mechanism under ideal conditions and when joint clearances exist. Finally, the influence of clearance size, driving speed, and material combination on the dynamics of the crank-slider mechanism is discussed based on motion parameters such as slider displacement, velocity, and acceleration curves, as well as Poincare maps.

Funding

This work is supported by the key research and Development Project of Shanxi province of China (Grant NO. 2022ZDYF082), Scientific and Technological Innovation Programs of Higher Education Institutions in Shanxi (Grant NO. 2022L708, 2023L563), the Opening Foundation of Shanxi Key Laboratory of Advanced Manufacturing Technology (Grant NO. XJZZ202105), the Fundamental Research Program of Shanxi Province(Grant No. 202303021211195) and the Lyuliang City High-level Science and Technology Talent Plan Special Project (Grant No. 2023RC17).

Conflicts of interest

The authors declare no conflict of interest.

Data availability statement

All data has already been reported in the manuscript.

Author contribution statement

Conceptualization, W.Y. and L.J.; Methodology, W.Y.; Software, L.J. and C.C; Validation, N.F.P, W.Y. and Z.L.; Formal Analysis, Z.L.; Investigation, W.Y.; Resources, W.Y. and L.H.; Data Curation, W.Y.; Writing – Original Draft Preparation, W. Y.; Writing – Review & Editing, W.Y., Z.L. and N.F.P.; Visualization, W.Y.; Supervision, N.F.P; Project Administration, W.Y.; Funding Acquisition, W.Y, L.J and L.H.

References

[1] E. Zakhariev, Dynamics of rigid multibody systems with clearances in the joints*, J. Mech. Struct. Mach. **27**, 63–87 (1999)
[2] C. Zhu, Z. Zhao, Research on influence of joint clearance on precision of 3-TPT parallel robot, J. Mech. Sci. **10**, 287–298 (2019)
[3] C.S. Liu, K. Zhang, R. Yang, The FEM analysis and approximate model for cylindrical joints with clearances, J. Mech. Mach. Theory. **42**, 183–197 (2007)
[4] A. Chaker, A. Mlika, M.A. Laribi et al., Clearance and manufacturing errors' effects on the accuracy of the 3-RCC spherical parallel manipulator, J. Eur. J. Mech. A-Solid. **37**, 86–95 (2013)
[5] I. Khemili, L. Romdhane, Dynamic analysis of a flexible slider-crank mechanism with clearance, J. Eur. J. Mech. A-Solid. **27**, 882–898 (2008)
[6] S. Erkaya, İ. Uzmay, Determining link parameters using genetic algorithm in mechanisms with joint clearance, J. Mech. Mach. Theory. **44**, 222–234 (2009)
[7] P. Flores, J. Ambrósio et al, Lubricated revolute joints in rigid multibody systems, J. Nonlinear. Dyn. **56**, 277–295 (2009)
[8] Z. Qi, X. Luo, Z. Huang, Frictional contact analysis of spatial prismatic joints in multibody systems, J. Multibody. Syst. Dyn. **26**, 441–468 (2011)
[9] Y. Zhao, Z.F. Bai, Dynamics analysis of space robot manipulator with joint clearance, J. Acta. Astronaut. **68**, 1147–1155 (2011)
[10] G. Wang, H. Liu, P. Deng, Dynamics analysis of spatial multibody system with spherical joint wear, J. Tribol. **137**, 021605 (2015)
[11] P. Flores, J. Ambrósio, J.C.P. Claro et al, Translational joints with clearance in rigid multibody systems, J.J. Comput. Nonlin. Dyn. **3**, 011007–1–10–0 (2008)
[12] F.F. Zhuang, Q. Wang, Modeling and analysis of rigid multibody systems with driving constraints and frictional translation joints, J. Acta. Mech. Sinica-Prc. **30**, 437–446 (2014)
[13] X. Wu, Y. Sun, Y. Wang et al, Dynamic analysis of the double crank mechanism with a 3D translational clearance joint employing a variable stiffness contact force model, J. Nonlinear. Dyn. **99**, 1937–1958 (2020)
[14] F. Marques, P. Flores, J.C.P. Claro et al., A survey and comparison of several friction force models for dynamic analysis of multibody mechanical systems, J. Nonlinear. Dynam. **86** 1407–1443 (2016)
[15] M. Qian, Z. Qin, S. Yan et al., A comprehensive method for the contact detection of a translational clearance joint and dynamic response after its application in a crank-slider mechanism, J. Mech. Mach. Theory **145** 103717 (2020)
[16] Y. Zhao, Z.F. Bai, Dynamics analysis of space robot manipulator with joint clearance, J. Acta. Astronaut. **68**, 1147–1155 (2011)
[17] S. Liu, Y. Cui, Y. Fu et al., Modeling of lubricated translational joints in rigid-partially flexible multibody systems and its application in two-stroke marine diesel engines, J. Tribol. Int. **165**, 107244 (2022)

[18] X. Chen, S. Jiang, Y. Deng, Dynamic responses of planar multilink mechanism considering mixed clearances, J. Shock. Vib. 2020, 1–18 (2020)
[19] X. Zheng, J. Li, Q. Wang, et al., A methodology for modeling and simulating frictional translational clearance joint in multibody systems including a flexible slider part, J. Mech. Mach. Theory. **142**, 103603 (2019)
[20] K.H. Hunt, F.R.E. Crossley, Coefficient of restitution interpreted as damping in vibroimpact, J. Appl. Mech-T. Asme. **42**, 440–445 (1975)
[21] C.S. Koshy, P. Flores, H.M. Lankarani, Study of the effect of contact force model on the dynamic response of mechanical systems with dry clearance joints: computational and experimental approaches, J. Nonlinear. Dynam. **73**, 325–338 (2013)
[22] Q. Tian, C. Liu, M. Machado, et al., A new model for dry and lubricated cylindrical joints with clearance in spatial flexible multibody systems, J. Nonlinear. Dynam. **64**, 25–47 (2011)
[23] S. Jiang, X. Chen, Reducing undesirable effects of clearances on dynamic and wear of planar multi-link mechanism, J. Nonlinear. Dynam. **100**, 1173–1201 (2020)

Cite this article as: Y. Wang, L. Juan, N. Fengping, C. Chao, Z. Lei, L. Hui, Dynamic analysis of crank slider mechanism considering 3D translational joint clearance based on variable contact area, Mechanics & Industry 26, 5 (2025), https://doi.org/10.1051/meca/2025001